Universidad Europea MADRID

TRABAJO FIN DE GRADO

Grado en Biotecnología

CHARACTERIZATION OF MACROPHAGE SUBPOPULATIONS LOCATED IN THE PERITONEAL SUBMESOTHELIAL SPACE

Autor/es: **Belén Álvarez Lázaro**

Villaviciosa de Odón, *Julio 2023*

ANEXO IX

Título del Trabajo: Characterization of macrophage subpopulations located in the peritoneal submesothelial space.

Este trabajo ha sido realizado en el laboratorio de Carlos Ardavín, Centro Nacional de Biotecnología, CSIC.

Tutor/es: Carlos Ardavín Castro y María Teresa Coiras López.

Table of content

1. List of abbreviations

CCR2	Chemokine receptor type 2
Ccr2$^{-/-}$	Chemokine receptor type 2 deficient
CSFR1	Colony-stimulating factor-1 receptor
CXCL13	C-X-C motif chemokine ligand 13
FALCs	Fat associated lymphoid clusters
GATA6	GATA binding protein 6
IgA	Immunoglobulin A
IgM	Immunoglobulin M
LPMs	Large peritoneal macrophages
LysM	Lysozyme M
LysM-GFP	Lysozyme M-Green fluorescent protein
Lyve-1	Lymphatic vessel endothelial hyaluronan receptor 1
M-CSF	Macrophage colony-stimulating factor
MerTK	MER proto-oncogene tyrosine kinase
MHCII	MHC class II
moCs	Monocyte-derived cells
resMØ-aggregates	Resident macrophage aggregates
SPMs	Small peritoneal macrophages
submes-MØs	Submesothelial macrophages
TGF-β	Transforming growth factor beta 1
Tim4	T-cell immunoglobulin and mucin-domain-containing molecule
WMI-CF	Whole-mount immunofluorescence and confocal microscopy

2. Abstract

Based on preliminary data revealing the existence of a macrophage layer in the connective tissue beneath the peritoneal mesothelium, in the present work submesothelial macrophages (submes-MØs) have been characterized by whole-mount immunofluorescence combined with confocal microscopy, as well as flow cytometry. Three main submes-MØ subpopulations were found in the submesothelial space of C57BL/6 mice in the steady state: Tim4^{+} MHCII^{low}, Tim4^{+} MHCII^{high} and Tim4^{-} MHCII^{high} submes-MØs. Differential expression of the resident peritoneal macrophage markers Tim4 and Gata6, and dependence on the chemokine receptor CCR2, support that Tim4^{+} MHCII^{low} and Tim4^{+} MHCII^{high} submes-MØs belong to the resident macrophage family and therefore have an embryonic origin. In contrast, Tim4^{-} MHCII^{high} submes-MØs would derive from adult bone marrow monocytes. Peritoneal *E. coli* infection promoted a transition from an elongated to a stellate morphology in submes-MØs, involving the formation of three-dimensional extensions that penetrated between mesothelial cells, suggesting that *E. coli* triggered submes-MØ activation. The contribution of the different submes-MØ subpopulations to defense against peritoneal infection remains to be investigated.

3. Introduction

3.1. The peritoneal cavity and the peritoneum

The peritoneal cavity is a virtual space, hostess to the abdominal organs (Liu et al., 2021) (Figure 1). In mice, in the steady state, it contains 50-100 µL of peritoneal fluid which is secreted by mesothelial cells and acts as a lubricant within the peritoneal cavity, preventing mechanical friction between the organs present in the abdomen (Zhang et al., 2019; Zindel et al., 2021). When the cavity homeostasis is disrupted, the peritoneal fluid volume increases (Ahmed et al., 2020), a condition called ascites (Szender et al., 2017). Two primary pathologies affect the peritoneal cavity: abdominal sepsis and metastatic tumor growth. These two conditions can be life-threatening because of the ease of tumor cells or pathogens to reach all intra-abdominal organs through the peritoneal cavity. Other important pathologies in the peritoneal cavity are abdominal injuries (in the parietal or visceral peritoneum, caused by trauma or surgery), loss of intestinal wall integrity (for example in appendicitis or ulcers), peritoneal endometriosis (proliferation of endometrial tissue in the cavity) and peritoneal autoimmune serositis (inflammation caused either by autoimmune diseases such as Chron's disease or by post-surgical peritoneal adhesions).

The peritoneal cavity is protected by 2 different lines of defense, a first one made up of resident peritoneal immune cells, free in the fluidic environment of the peritoneal cavity, and a second one made up of immune cells forming lymphoid aggregates, or fat-associated lymphoid clusters (FALCs), within abdominal adipose tissues, such as the omentum, mesentery or gonadal fat. The first one is composed mainly of resident peritoneal macrophages (or LPMs) and B1 cells. On the other hand, FALCs are composed of B cells, T cells and myeloid cells, supported by a fibroblastic stromal cell network, and operate like secondary lymphoid tissues. When homeostasis is disrupted, such as in infection, FALCs of the omentum (called milky spots) can recruit T and B cells and mount antigen-specific immune responses (van Baal et al., 2017).

The peritoneum is the serous membrane that covers the peritoneal cavity. It is the largest serous membrane of the human body. The parietal face delineates the internal surface of the abdominal wall (Figure 2), while the visceral face lines with the serosal layer of abdominal organs. The peritoneum is composed by the

mesothelium (in contact with the peritoneal cavity), a basal membrane and a submesothelial connective tissue (van Baal et al., 2017). Abdominal organs are connected to the abdominal wall thanks to a double fold of the peritoneum known as the mesentery which also holds blood vessels, nerves and lymphatic vessels.

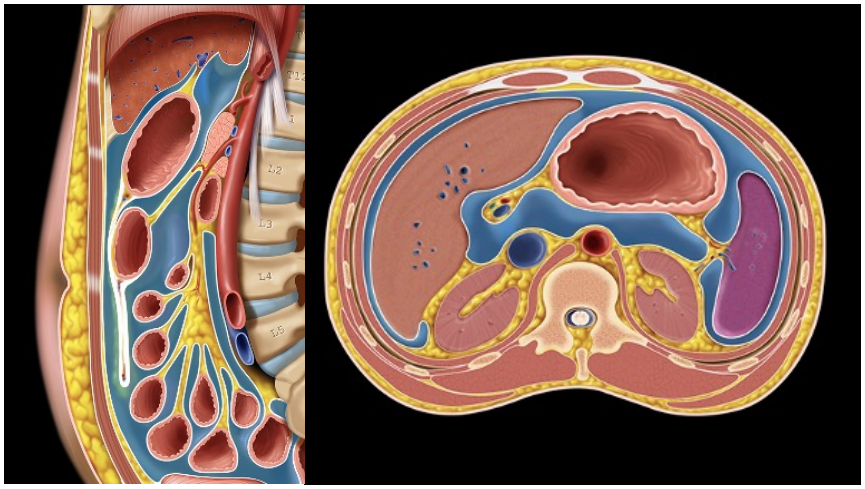

Figure 1: Sagittal and transversal sections of the abdomen showing the peritoneal cavity (in blue). Adapted from (Imaging Approach to the Peritoneum, Mesentery, and Abdominal Wall | Radiology Key, 2016).

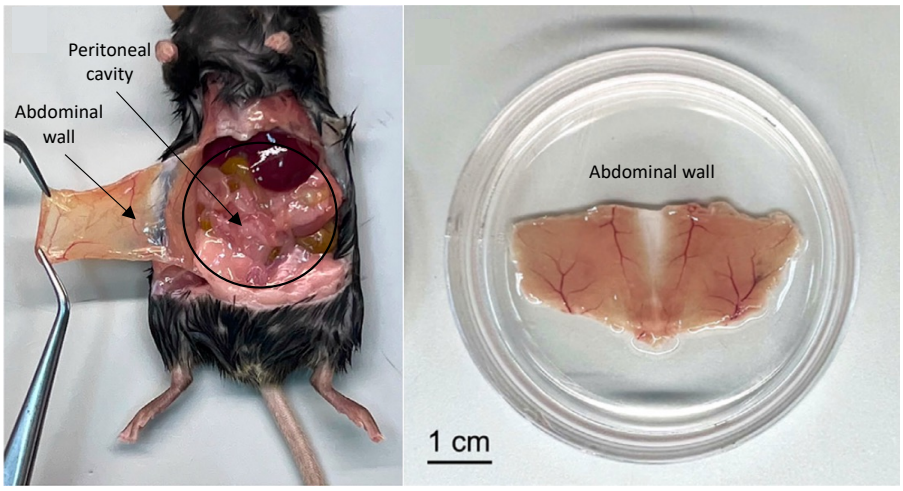

Figure 2: Mouse abdominal wall and peritoneal cavity. Adapted from Ferriz et al., 2023.

3.2. The mesothelium

The mesothelium is a monolayer composed of mesothelial epithelial cells of mesodermal origin, which is in contact with the peritoneal cavity (Figure 3). Mesothelial cells are connected through tight junctions, desmosomes, and gap junctions. A basal membrane consistent of an extracellular matrix mostly made of collagen and laminin holds the cells (Figure 4).

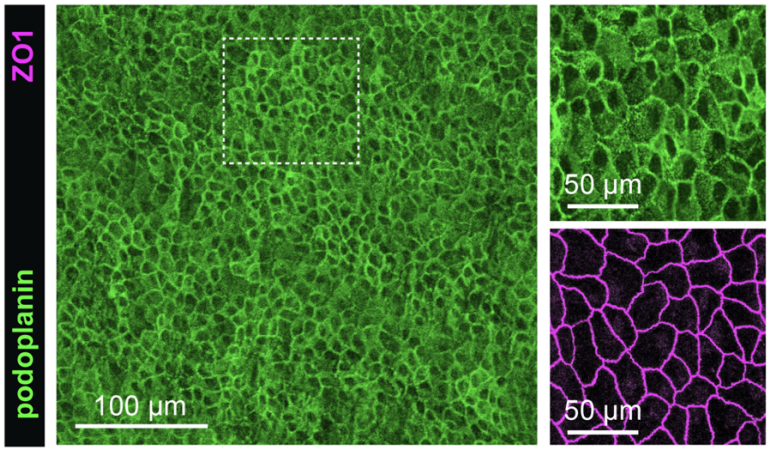

Figure 3: Whole-mount immunofluorescence and confocal microscopy of the mesothelium under normal conditions (Vega-Pérez et al., 2021).

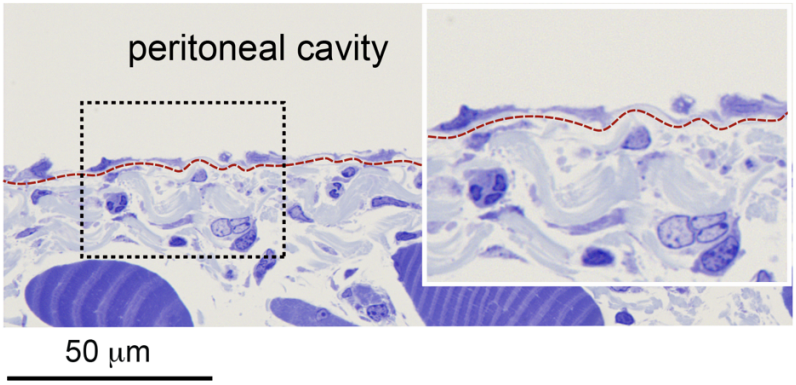

Figure 4: Section of a non-infected peritoneal wall, red line: mesothelial basal membrane (Vega-Pérez et al., 2021).

3.3. The peritoneal cavity immune system

In steady state, LPMs and B1 cells are the most abundant populations in the peritoneal cavity. LPMs and B1 cells represent around 50% and 30% of peritoneal immune cells, respectively. The remaining 20% is made up of T cells, small peritoneal macrophages (SPMs), NK cells, and mast cells (Bain & Jenkins, 2018).

3.3.1. Peritoneal macrophages

Peritoneal macrophages can be divided into two populations according to the expression of F4/80 and MHC class II (MHCII): F4/80^{hi} MHCII^{-} LPMs and F4/80^{lo} MHCII^{+} SPMs. LPMs express tissue-resident macrophage receptors, such as CD64, CD14 and MerTK (MER proto-oncogene, tyrosine kinase), and cavity macrophage markers, such as the scavenger receptor Tim4 (T-cell

immunoglobulin and mucin-domain-containing molecule), CSFR1 (colony-stimulating factor-1 receptor) which is the receptor for M-CSF (macrophage colony-stimulating factor), and the transcription factor GATA6 (GATA binding protein 6) (Bain & Jenkins, 2018). LPMs are long-lived cells that are generated during embryonic life from yolk sac macrophages and fetal liver monocytes, and are maintained by self-renewal during adult life. By contrast, SPMs arise from bone marrow-derived monocytes and exhibit a rapid turnover rate (Salm et al., 2023).

The main tissue-specific transcription factor LPMs depend on is GATA6, which is involved in the differentiation and survival of LPMs. GATA6 is activated by retinoic acid, claimed to be mainly produced in the omentum (Okabe & Medzhitov, 2014).

LPMs were initially thought to be responsible for pathogen clearance but research performed over the last years have revealed that they also fulfill peritoneal homeostatic and repair functions. In this regard, LPMs have been shown to clear apoptotic cells through dead cell recognition receptors, such as CD36, CD93, CD163, Tim4, and MerTK (Gautier et al., 2012; Nishi et al., 2014).

3.3.2. B-1 cells

B1 cells in the peritoneal cavity and omentum depend on the chemokine CXCL13 (C-X-C motif chemokine ligand 13). This chemokine allows B1 cells to migrate from the circulation to the cavity where they produce IgM (immunoglobulin M), one of the first lines of defense against many pathogens. B1 cells can also travel to the intestine and secrete IgA (immunoglobulin A) which has an essential control of the intestinal microbiota (Smith & Baumgarth, 2019). The secretion of IgA by B1 cells is dependent on TGF-β (transforming growth factor beta 1), which is secreted by LPMs (Okabe & Medzhitov, 2014). B1 cells are continuously moving to the omentum, to the peritoneal cavity and back to the omentum (Berberich et al., 2007; Mark Ansel K., 2002).

3.4. The omentum

The omentum (Figure 5) is a visceral adipose tissue which derives from the mesentery and is connected to the spleen, stomach, pancreas, and colon (Meza-Perez & Randall, 2017). This organ contains milky spots, which connect

to the peritoneal cavity through discontinuities in the mesothelial layer, facilitating the translocation of leukocytes from the omentum to the cavity and vice versa. In the peritoneal cavity, leukocytes perform vital functions associated with the maintenance of homeostasis and repairing of damaged tissue. When the cavity homeostasis is disrupted such as in inflammation, infection or tumor metastasis, peritoneal leukocytes are recruited to the omentum (Liu et al., 2021).

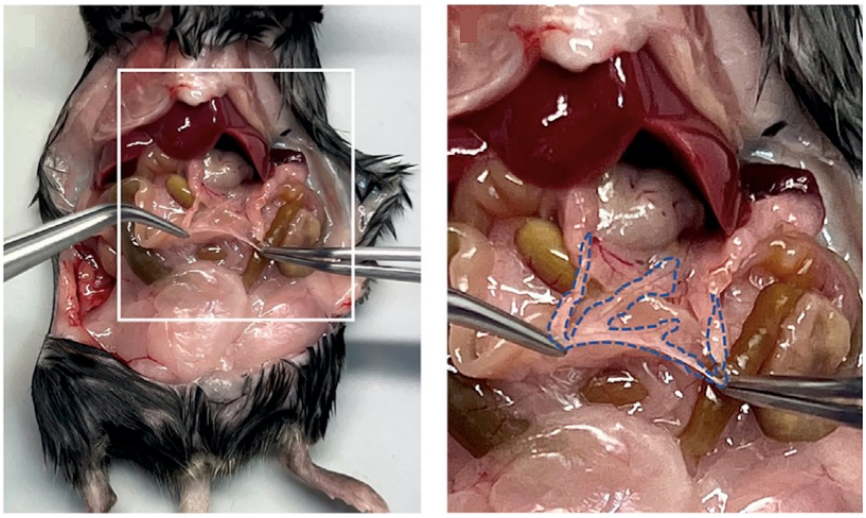

Figure 5: Close-up of a mouse omentum (Ferriz et al., 2023).

3.5. Immune response to infection in the peritoneal cavity

The homeostasis of the peritoneal cavity can be altered leading to infection by different stimuli such as the rupture of the abdominal wall by surgery, trauma, appendicitis, or ulcers (Capobianco et al., 2017). Infection in the peritoneal cavity can be hazardous because of the ease of pathogens to reach the bloodstream. The innate immune system has a pivotal role in the control of pathogens and their spreading to the rest of the body (Reim et al., 2011).

LPMs in homeostasis have been typically associated with apoptotic cell clearance as well as controlling the peritoneal fluid surfactant, among other functions. Under pathological conditions, extracellular signals promote a functional transition in LPMs, leading them to acquire an inflammatory phenotype which provides them with the capacity to perform defense roles against pathogens. In the case of infection, LPMs have the ability to phagocytose bacteria and to produce proinflammatory mediators (Wynn & Vannella, 2016), although the role of LPMs against in vivo microbial peritoneal infections remains largely

unknown. Depletion of LPMs through the administration of clodronate-loaded liposomes in experiments involving infection by *Escherichia coli*, *Acinetobacter baumannii* and *Enterococcus faecium*, led to a significant increase in bacterial burden and reduced survival in mice (Harris et al., 2019; Leendertse et al., 2009; Vega-Pérez et al., 2021). These findings confirm the crucial involvement of LPMs in bacterial clearance.

The functional relevance of LPMs in defense against peritoneal bacterial infection has been recently described in a report by the group of Carlos Ardavín showing that LPMs fulfill a crucial role in defense against bacterial infection through the formation of resMØ-aggregates (from resident macrophages aggregates) (Vega-Pérez et al., 2021). Experiments based on whole mount immunofluorescence (WMI) and confocal microscopy techniques revealed that resMØ-aggregates attach to the inner face of the peritoneal wall as well as the omentum, providing a physical scaffold which enables the recruitment and interaction of immune cells within the peritoneal cavity. LPMs, B1-cells, neutrophils, and monocyte-derived cells (moCs) predominantly compose resMØ-aggregates that harbor a fibrin network, which plays a crucial role acting as the bond that makes the formation of the aggregate possible. The formation of resMØ-aggregates in response to *E.coli* is represented in Figure 6.

In later phases of infection, the dissolution of resMØ-aggregates via fibrinolysis is necessary, which is essentially performed by monocyte-derived macrophages leading to the resolution of inflammation (Vega-Pérez et al., 2021).

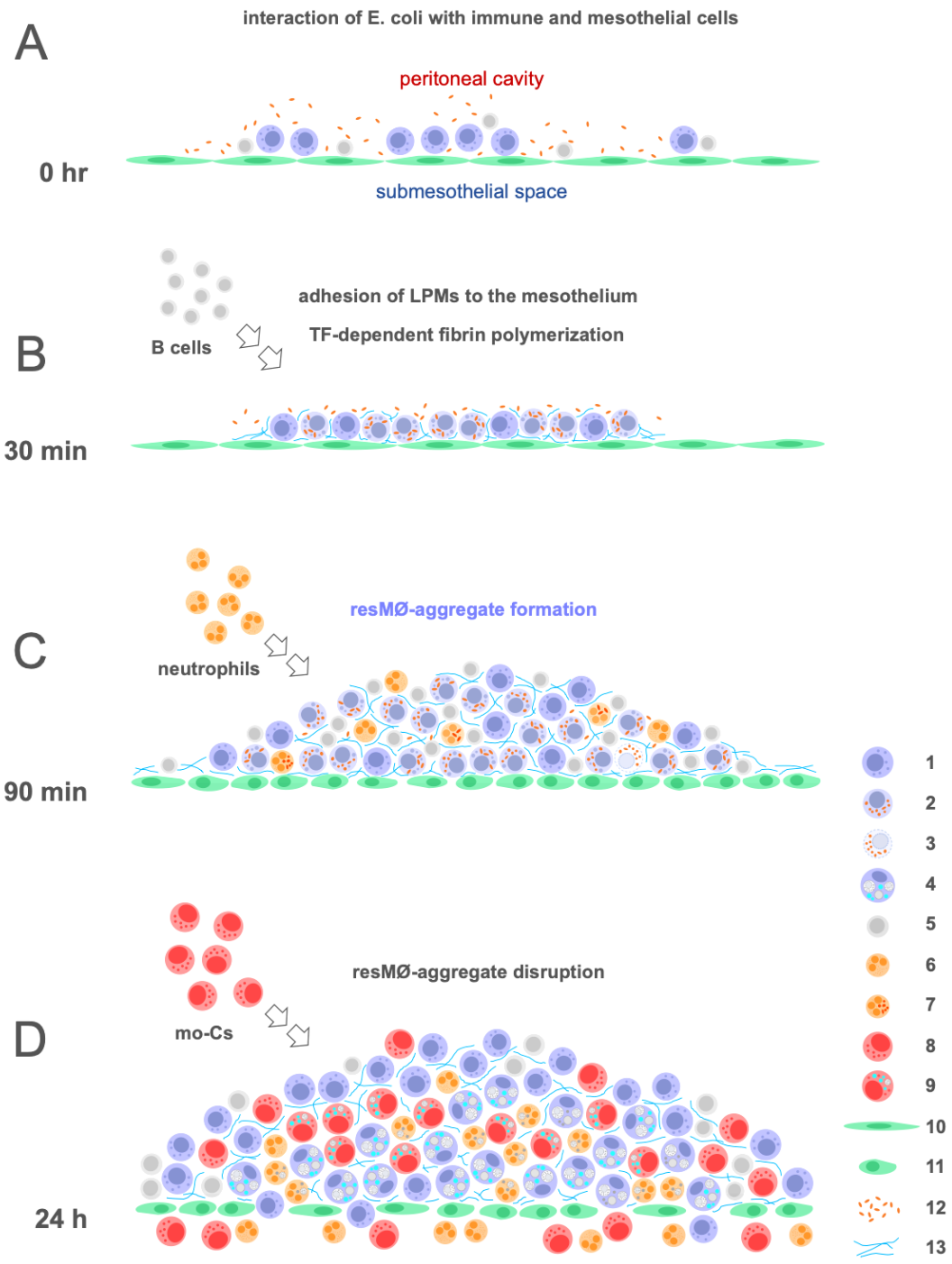

Figure 6: Formation of fibrin-dependent resident macrophage aggregates (resMØ-aggregates) in response to E.coli infection. 1: LPMs; 2: LPMs containing bacteria; 3: necrotic LPMs containing bacteria; 4: LPMs containing dead cells and fibrin; 5: moCs; 6: moCs containing dead cells and fibrin; 7: B cells; 8: neutrophils; 9: neutrophils containing bacteria; 10: neutrophils containing dead cells; 11: activated mesothelial cells; 12: bacteria; 13: fibrin. Image adapted from Ardavín et al., 2023; Vega-Pérez et al., 2021.

3.6. Submesothelial macrophages

WMI and confocal microscopy studies of the peritoneal wall performed in Carlos Ardavin's lab with the aim of exploring the role of the innate immune system of the peritoneal cavity in defense against bacterial infection, revealed the existence of a F4/80^{+} macrophage network located in the submesothelial space, whose function remains largely unknown. In this regard, submesothelial LysM^{+} resident peritoneal macrophages were described to contribute to tissue damage repair after laser-induced focal mesothelial injury (Uderhardt et al., 2019). Besides, two F4/80^{+} CD206^{+} macrophages subsets have recently been described in the peritoneal wall and serosa based on their differential lymphatic vessel endothelial hyaluronan receptor 1 (Lyve-1) and MHCII expression: Lyve-1^{high} MHCII^{low} and Lyve-1^{low} MHCII^{high} macrophages (Zhang et al., 2021).

4. Objectives

In this context, the main objective of the present work is to characterize the subpopulations of macrophages located in the submesothetial space and their response to peritoneal bacterial infection.

For this purpose, the following secondary objectives have been performed:

1. Characterization of macrophages subpopulations in the peritoneal submesothelial space.
2. Association between the expression of different receptors and the origin of the macrophages in the peritoneal submesothelial space.
3. Analysis of the contribution of the submesothelial macrophages to the defense against bacterial infections.

5. Methods

The experiments performed in this work mainly rely on two experimental strategies, as shown in Figure 7.

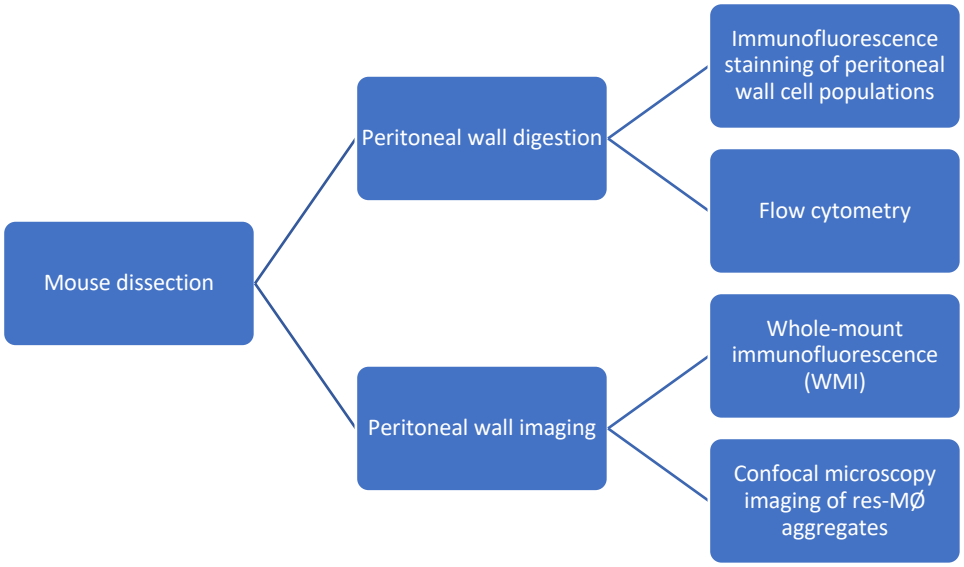

Figure 7: Diagram of the principal methods.

5.1. Mice

C57BL/6 mice were purchased from Charles River (L'Arbresle, France); $Ccr2^{-/-}$ mice in a C57BL/6 genetic background were kindly supplied by Dr. F. Tacke (RW-TH-University Hospital Aachen, Germany). Mice were housed at the Animal Facility of CNB/CSIC, on a 12h/12h light/dark cycle, with free access to food and water. Littermates of the same sex were randomly assigned to experimental groups. All the experiments were approved by the Animal Care and Use Committee of the Centro Nacional de Biotecnología-CSIC, Madrid, under the protocol 363/15.

5.2. Intraperitoneal infection with *Escherichia coli*

Mice were intraperitoneally infected with 1 x 10^7 colony-forming units of *Escherichia coli* strain M6L4, isolated from the mouse intestine and kindly provided by Dr. G. Núñez, University of Michigan Medical School, Ann Arbor, Michigan, USA. Mice were daily monitored for health and survival following the institutional guidance. Bacteria were grown overnight in LB plates at 37º C. Then

an isolated colony was incubated in liquid LB until stationary phase was reached and serial dilutions were made to obtain the desired inoculum. Analyses were performed 4 h post-injection.

5.3. Whole-mount immunofluorescence and confocal microscopy imaging for the peritoneal wall

Abdominal wall samples were dissected and fixed in 4% paraformaldehyde solution for 5 min at 4º C and washed twice with PBS. Samples were cut through the abdominal midline and each half was incubated in PBS 2% BSA for 30 min at 4º C to prevent unspecific binding of primary antibodies. Samples were incubated with fluorophore-conjugated antibodies and DAPI (Sigma-Aldrich) (Supplementary information: Table 1) in PBS 2% w/v BSA overnight at 4º C under shaking in the darkness. Samples were then washed with PBS for 5 min and mounted in µ-Dish 35 mm dishes (ibidi) with Mowiol-based WMI mounting solution, prepared as described in Ferriz et al., 2023. An in-house designed aluminum weight (Figure 8) was used to flatten the wall for optimal imaging. Images were acquired on a multispectral Leica Stellaris 5 confocal microscope (Leica microsystems) and data were analyzed using Image J software (NIH).

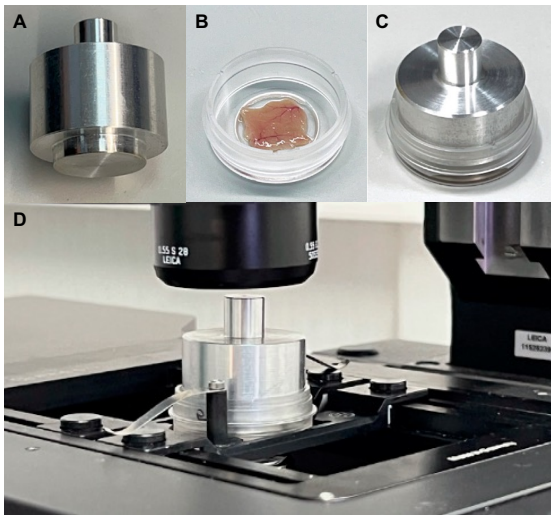

Figure 8: Mounting of peritoneal wall samples for WMI and confocal microscopy imaging. (A) Aluminum weight (B) Peritoneal wall sample transferred to a µ-Dish 35 mm dish containing mowiol-based WMI mounting solution (C) Peritoneal wall sample mounted in a µ-Dish 35 mm dish and an aluminum weight on top (D) Peritoneal wall sample mounted in a µ-Dish 35 mm dish with aluminum weight on top, placed on the stage of a confocal microscope. Adapted from Ferriz et al., 2023.

5.4. Processing of the peritoneal wall for flow cytometry

Peritoneal wall samples were placed facing the visceral peritoneum up in a 60-mm Petri dish and washed with PBS1x. Samples were then digested with 0.18 mg/mL Liberase TM (Roche), 0.04 mg/mL DNAse I (Roche) and 0.5 mg/mL Collagenase A (Roche) in RPMI 1640 w/o glutamine (Biowest) for 40 min at 37ºC, shaking the dish every 10 minutes. The enzymatic digestion was stopped with a solution containing 10% v/v FBS (Sigma-Aldrich), 0.04 mg/mL DNAse I (Roche) and RPMI (Biowest). The peritoneal surface was then carefully scraped off with the help of a single edge carbon steel blade (Electron Microscopy Science), while adding enzymatic digestion stop solution, to detach the cells located in the submesothelial space. The resulting cell suspensions was filtered through a 40-µm cell strainer (Pluriselect) and transferred into a 50mL Falcon. Samples were then resuspended in PBS-EDTA 3% FBS after erythrocyte lysis by osmotic shock and filtered through a 30-µm cell strainer (Sysmex) to remove cell debris. Fc receptors were blocked in a 96-well V-bottom plate with an anti-CD16/32 antibody at 4º C for 15 min and cells were subsequently stained with fluorophore-conjugated antibodies listed in Table 1 at 4º C for 20 min.

Data were acquired using a Becton Dickinson LSR II flow cytometer (BD Biosciences) and analyzed with FlowJo X software (Tree Star, Ashland, OR)

6. Results

6.1. Characterization of submesothelial macrophage subpopulations.

Imaging of the inner face of the peritoneal wall of C57BL/6 mice, in steady state, was performed by whole-mount immunofluorescence and confocal microscopy (WMI-CF), after immunofluorescent staining with antibodies against cell surface markers previously used to define macrophage subsets located in the peritoneal cavity (Vega-Pérez et al., 2021) or in the peritoneal serosa (Zhang et al., 2021), namely the scavenger receptor Tim4, MHCII molecules and the lymphatic endothelial marker Lyve-1, also expressed by perivascular macrophages (Hwee Ying Lim et al., 2018).

2-color immunofluorescent staining with anti-Tim4 antibodies and anti-podoplanin antibodies recognizing mesothelial cells, revealed the presence of $Tim4^{+}$ macrophages in the submesothelial space, a connective tissue layer that extends from the mesothelium to the skeletal muscle fibers forming the abdominal wall musculature; $Tim4^{+}$ macrophages, were arranged in a parallel array following muscle fibers (Figure 9A). The submesothelial location of these macrophages was confirmed by three dimensional images (3D-images) of the peritoneal wall (Figure 9B).

With the aim of exploring whether submesothelial macrophages comprised different subpopulations, imaging of the submesothelial compartment of the peritoneal wall performed after 3-color immunofluorescent staining with anti-Tim4, anti-MHCII and anti-Lyve-1 antibodies allowed the identification of three main subpopulations of submesothelial macrophages (submes-MØs): $Tim4^{+}$ $MHCII^{low}$ $Lyve\text{-}1^{high}$ submes-MØs, $Tim4^{+}$ $MHCII^{intermediate\text{-}high}$ $Lyve\text{-}1^{low}$ submes-MØs and $Tim4^{-}$ $MHCII^{high}$ $Lyve\text{-}1^{-}$ submes-MØs, hereafter $Tim4^{+}$ $MHCII^{low}$ submes-MØs, $Tim4^{+}$ $MHCII^{high}$ submes-MØs and $Tim4^{-}$ $MHCII^{high}$ submes-MØs (Figure 9C). A minor population of $Tim4^{-}$ $MHCII^{high}$ $Lyve\text{-}1^{+}$ submes-MØs was also detectable (not shown).

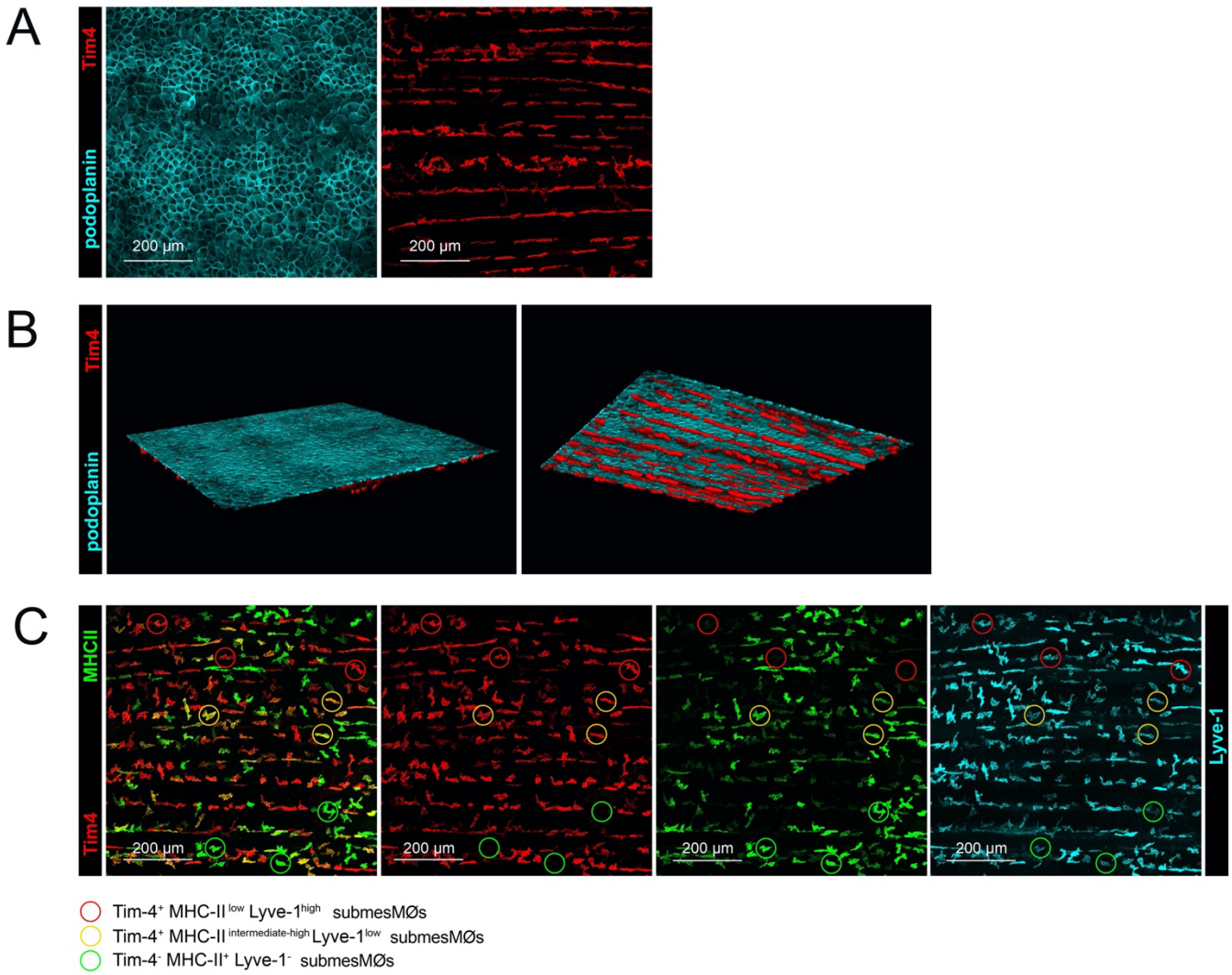

Figure 9: ***Characterization of submesothelial macrophages****.* ***A****. WMI-CF imaging of the peritoneal wall, after 2-color immunofluorescent staining with anti-Tim4 and anti-podoplanin antibodies, revealing the existence of Tim4⁺ macrophages located underneath the mesothelium, defined by the expression of podoplanin.* ***B****. 3D-images of the same area analyzed in A, showing the upper (left) and lower (right) faces of the peritoneal wall.* ***C****. WMI-CF imaging of the submesothelial compartment of the peritoneal wall of C57BL/6 mice, after 3-color immunofluorescent staining with anti-Tim4, anti-MHCII and anti-Lyve-1 antibodies. Examples of Tim4⁺ MHCII^{low}, Tim4⁺ MHCII^{high} and Tim4⁻ MHCII^{high} submes-MØs are marked by red, yellow, and green circles, respectively.*

6.2. CCR2-dependence of submes-MØ subpopulations

Flow cytometry analyses of cell suspensions of the submesothelial tissue, obtained by enzymatic digestion of the peritoneal wall, followed by gentle scraping of the side facing the peritoneal cavity and filtering through a 40µm cell strainer, confirmed the existence of the submes-MØ subpopulations previously defined on the basis of WMI-CF studies (Figure 10A and 10B). It is important to note that processing peritoneal wall samples for flow cytometry caused a partial Lyve-1 downregulation, most likely due to an activation-induced cleavage of this molecule, as described in in vitro assays (Johnson et al., 2007), resulting in a lower Lyve-1 expression by Tim4^{+} MHCII^{low} and Tim4^{+} MHCII^{high} submes-MØ subsets than expected, based of WMI-CF analyses (Figure 10B). Interestingly, as shown in Figure 10C, Tim4^{+} MHCII^{low} and Tim4^{+} MHCII^{high} submes-MØs, but not Tim4^{-} MHCII^{high} submes-MØs, expressed Gata6, a transcription factor controlling LPM-specific gene expression proliferation and survival (Gautier et al., 2014).

The expression of the LPM markers Tim4 and Gata6 by Tim4^{+} MHCII^{low} and Tim4^{+} MHCII^{high} submes-MØs supports that they are resident macrophages, whereas Tim4^{-} MHCII^{high} submes-MØs are monocyte-derived macrophages. To address this issue, submes-MØ subpopulations were analyzed by flow cytometry in CCR2-deficient (Ccr2$^{-/-}$) mice, in which monocyte egress from the bone marrow and recruitment to inflammatory areas is blocked (Shi & Pamer, 2011). According to this hypothesis, Tim4^{-} MHCII^{high} submes-MØs were strongly reduced in Ccr2$^{-/-}$ mice, whereas Tim4^{+} MHCII^{high} submes-MØs were not affected, and Tim4^{+} MHCII^{low} submes-MØs increased (Figure 10D-10E). These results were confirmed by WMI-CF imaging of the submesothelial compartment of the peritoneal wall, showing a marked reduction in Tim4^{-} MHCII^{high} submes-MØs and an increase in and Tim4^{+} MHCII^{low} submes-MØs (Figure 10F).

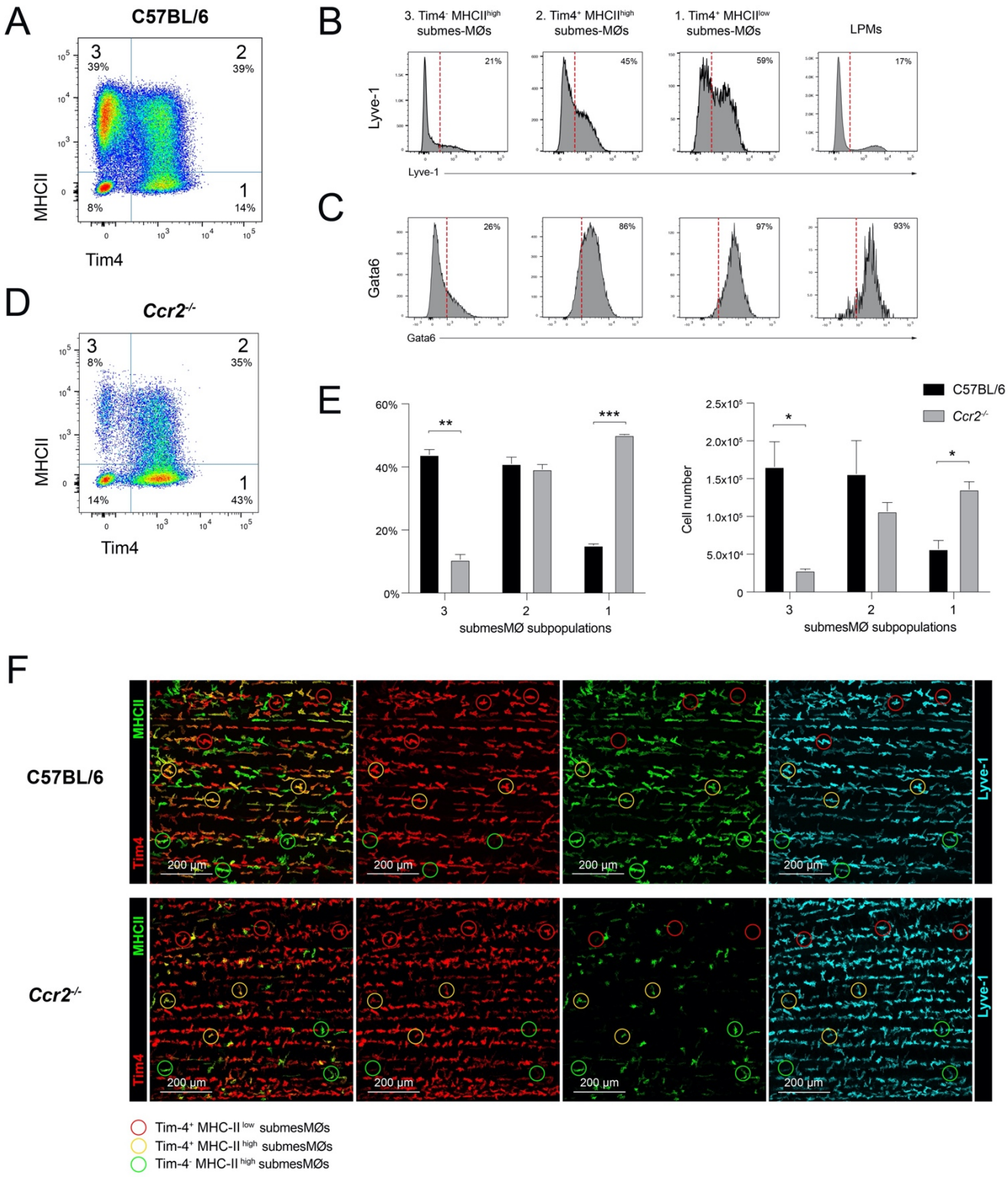

*Figure 10: **Effect of CCR2 deficiency on submes-MØ subpopulations**. **A** and **D**. Flow cytometry analysis of submesothelial tissue cell suspensions from C57BL/6 (**A**) and Ccr2$^{-/-}$ (**D**) mice, showing the Tim4 versus MHCII profile after gating for CD45^{+} CD11b^{+} CD19^{-} CD90^{-} Ly6G^{-} cells. Quadrants 1, 2 and 3 correspond to Tim4^{+} MHCII^{low}, Tim4^{+} MHCII^{high} and Tim4^{-} MHCII^{high} submes-MØ subpopulations, respectively. The percentage of each subpopulation, considering as 100% the sum of the 3 subpopulations, is indicated. **B** and **C**. Lyve-1 (**B**) and Gata6 (**C**) expression of the indicated cell populations. The percentage of cells above background staining (indicated by a red dotted line) is shown. **E**. Relative percentage and cell number of Tim4^{+} MHCII^{low} (1), Tim4^{+} MHCII^{high} (2) and Tim4^{-} MHCII^{high} (3) submes-MØ subpopulations, in C57BL/6 and Ccr2$^{-/-}$ mice. **F**. WMI-CF imaging of the submesothelial compartment of the peritoneal wall of C57BL/6 and Ccr2$^{-/-}$ mice, after 3-color immunofluorescent staining with anti-Tim4, anti-MHCII and anti-Lyve-1 antibodies. Examples of Tim4^{+} MHCII^{low}, Tim4^{+} MHCII^{high} and Tim4^{-} MHCII^{high} submes-MØs are marked by red, yellow and green circles, respectively.*

6.3. Response of submes-MØs to peritoneal E. coli infection

As pointed out in the Introduction section, previous work from Carlos Ardavin's lab demonstrated that LPMs play a crucial role in defense against *E. coli* infection by fulfilling an efficient bacterial clearance through the formation of mesothelium-bound macrophage aggregates (Vega-Pérez et al., 2021). In order to assess how submes-MØs responded to *E. coli* infection, imaging of the submesothelial compartment was performed by WMI-CF, at 4 hr after intraperitoneal *E. coli* injection. *E. coli* infection led to a complete loss of Lyve-1 expression in Tim4^{+} MHCII^{low} and Tim4^{+} MHCII^{high} submes-MØ subpopulations, and to a significant increase in Tim4^{+} MHCII^{high} submes-MØs paralleled by a decrease in Tim4^{+} MHCII^{low} submes-MØs (Figure 11A). Accordingly, the analysis by flow cytometry of submesothelial tissue cell suspensions revealed that *E.coli* infection caused a strong MHCII upregulation of Tim4^{+} MHCII^{low}, Tim4^{+} MHCII^{high} and Tim4^{-} MHCII^{high} submes-MØs, leading to a marked increase in Tim4^{+} MHCII^{high} submes-MØs, paralleled by the almost complete loss of Tim4^{+} MHCII^{low} submes-MØs (Figure 11B). Noteworthy, *E. coli* infection induced a pronounced change in submes-MØ cell shape that changed from an elongated to a stellated morphology (Figure 11C). Moreover, 3D-images of the upper and lower faces of the peritoneal wall, obtained after 3-color immunofluorescent staining with anti-Tim4, anti-MHCII and anti-podoplanin antibodies (Figure 12), revealed that *E. coli* infection promoted the formation of long three-dimensional extensions, particularly by Tim4^{-} MHCII^{high} submes-MØs, that penetrated between mesothelial cells, and therefore gained access to the peritoneal cavity (Figure 12; lower left panel).

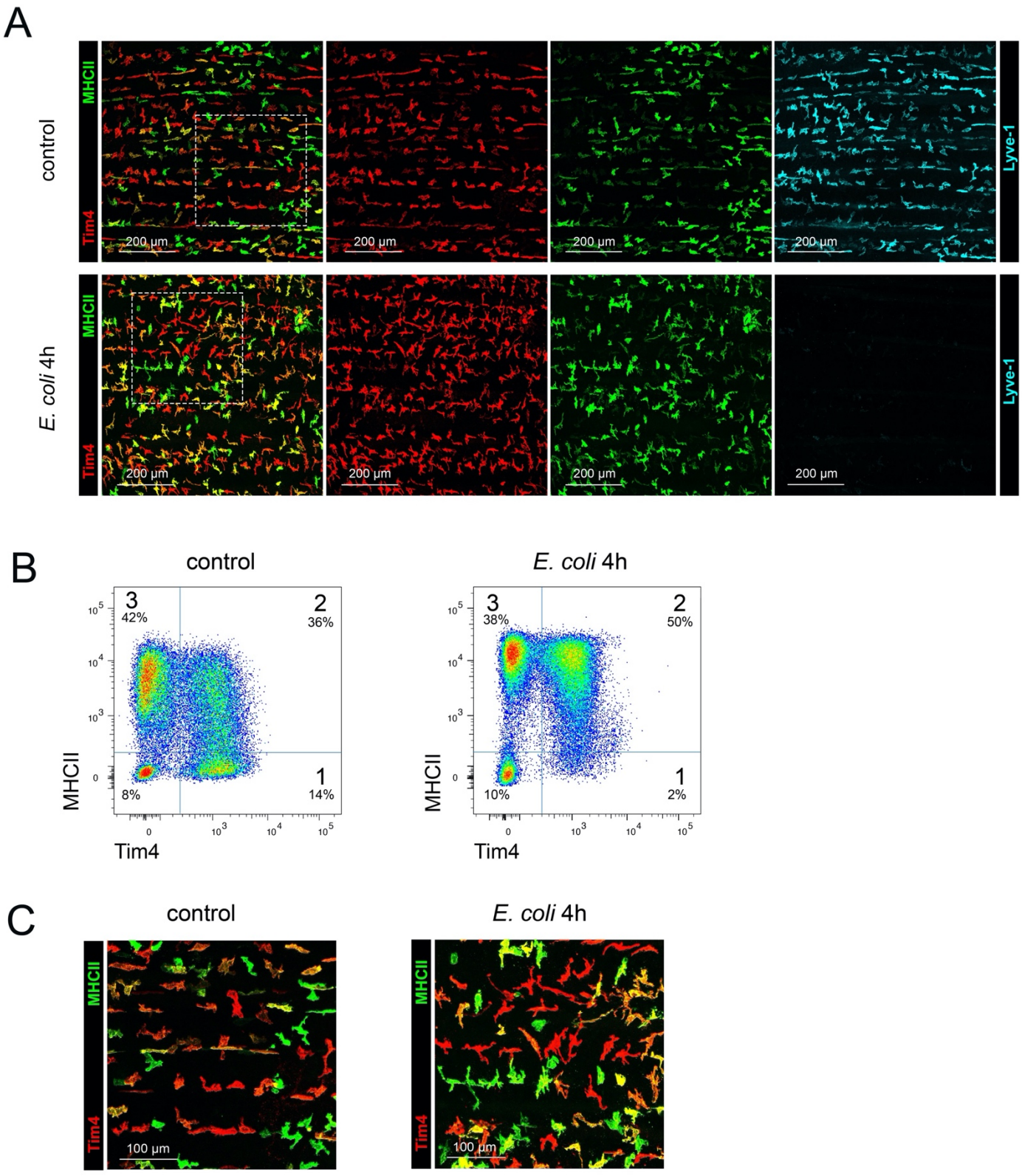

Figure 11: ***Response of submes-MØs to peritoneal E. coli infection****.* ***A****. WMI-CF imaging of the submesothelial compartment of the peritoneal wall in control mice and at 4hr after E. coli infection, after 3-color immunofluorescent staining with anti-Tim4, anti-MHCII and anti-Lyve-1 antibodies.* ***B.*** *Flow cytometry analysis of submesothelial tissue cell suspensions from control mice and at 4hr after E. coli infection, performed as described for Figures 2A and 2D.* ***C.*** *Enlargement of the square areas marked with a white dotted line in A.*

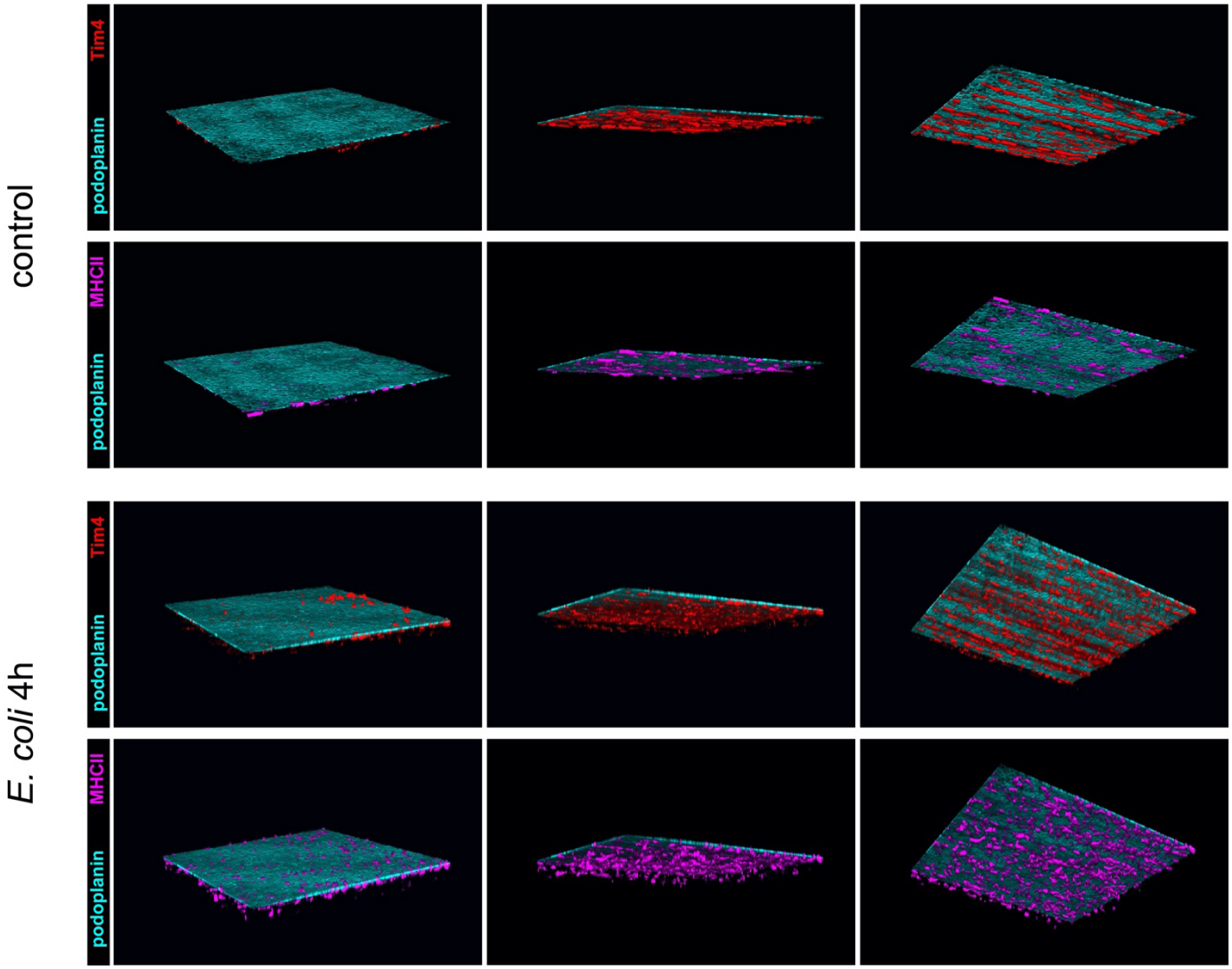

Figure 12: ***Effect of E. coli infection in the morphology of submes-MØs****. 3D-images of the upper and lower faces of the peritoneal wall, of control mice and mice at 4 hr after E. coli infection, obtained after 3-color immunofluorescent staining with anti-Tim4, anti-MHCII and anti-podoplanin antibodies.*

7. Discussion

Previous analyses by WMI + CF performed in Carlos Ardavin's lab, and aiming at addressing the role of LPMs against intraperitoneal bacterial infection, revealed the existence of F4/80^{+} macrophages in the connective tissue located underneath the mesothelium of the peritoneal wall. In order to characterize these submesothelial macrophages (submes-MØs), in this study we have relied on a number of cell surface markers recently used to address the functional relevance of resident peritoneal macrophages (Vega-Pérez et al., 2021; Zhang et al., 2021), namely, Tim4, MHCII and Lyve-1. Tim4 is expressed by LPMs and resident macrophages located in other body cavities, such as those present in the pleural and pericardiac cavities (Bain & Jenkins, 2018; Buechler et al., 2019). Lyve-1, originally described as a lymphatic vessel marker (Jackson et al., 2001) has been recently reported to be expressed by perivascular macrophages in different tissues, such as the heart, fat, dermis, and lung (Chakarov et al., 2019; Hwee Ying Lim et al., 2018). Interestingly, two macrophage subsets associated to the peritoneal serosa have been recently described based on their differential Lyve-1 and MHCII expression: Lyve-1^{hi} MHCII$^{lo\text{-}hi}$ and Lyve-1$^{lo/-}$ MHCII^{hi} macrophages (Zhang et al., 2021).

Our data revealed the existence of three main subpopulations of macrophages located in the submesothelial space of the peritoneal wall: Tim4^{+} MHCII^{low} Lyve-1^{high}, Tim4^{+} MHCII$^{intermediate\text{-}high}$ Lyve-1^{low} and Tim4^{-} MHCII^{+} Lyve-1^{-} submes-MØs, hereafter Tim4^{+} MHCII^{low}, Tim4^{+} MHCII^{high} and Tim4^{-}MHCII^{high} submes-MØs.

The existence of a network of submesothelial macrophages was previously described in a report by Ron Germain's lab analyzing the response of submesothelial macrophages to laser-induced micro injuries. Submesothelial macrophages were identified on the basis of the expression of lysozyme M (LysM), using LysM-GFP (lysozyme M-green fluorescent protein) mice, but neither their phenotype nor the existence of different submes-MØs subsets was addressed in this report (Uderhardt et al., 2019). On the other hand, the fact that the two serosal macrophage subsets described by Gwendalyn Randolph's group (Zhang et al., 2021) were defined based on their mutually exclusive expression of Lyve-1 and MHCII, suggests that they could be related to the submes-MØ

subpopulations described in the present study. However, additional analyses would be required to address this issue, since the expression of Tim4, a key marker for the characterization of submes-MØ subpopulations, was not taken into account when defining serosal macrophages subsets.

Macrophages present in the peritoneal cavity fluid, in the steady state, comprise Tim4^{+} MHCII^{low} Gata6^{+} LPMs, and Tim4^{-} MHCII^{high} Gata6^{-} SPMs. LPMs are tissue-resident macrophages, generated during embryonic life from yolk sac macrophages and fetal liver monocytes, that are essentially maintained by self-renewal; in contrast, SPMs derive from bone marrow monocytes and have a high turnover rate (Bain & Jenkins, 2018). Consequently, Tim4^{+} MHCII^{low} Lyve-1^{high} and Tim4^{+} MHCII$^{intermediate-high}$ Lyve-1^{low} submes-MØs, that both express the transcription factor Gata6, and do not undergo a reduction in Ccr2$^{-/-}$ mice, most likely correspond to resident submes-MØ subpopulations. However, their potential relation with LPMs and whether they originate from embryonic progenitors remains to be addressed. On the other hand, the increase in Tim4^{+} MHCII^{low} Lyve-1^{high} submes-MØs found in Ccr2$^{-/-}$ mice might reflect that these cells fill the empty niche left by Tim4^{-} MHCII^{+} Lyve-1^{-} submes-MØs. Our data on the phenotype and CCR2-dependence of Tim4^{-} MHCII^{high} submes-MØs support that they are continuously generated from bone marrow monocytes recruited to the submesothelial compartment.

As pointed out above, upon laser-induced injury in the peritoneal serosa, submesothelial LysM^{+} macrophages were reported to contribute to tissue repair by extending pseudopods towards the damaged area, acquiring a stellate morphology (Uderhardt et al., 2019). In this regard, the morphological changes underwent by submes-MØs induced by *E. coli* infection might reflect that they become activated and consequently might contribute to defense against infection. In favor of this hypothesis, *E. coli* infection-triggered loss of Lyve-1 expression by submes-MØs most likely resulted from submes-MØ activation, since activation-induced proteolytic cleavage of Lyve-1 has been reported (Johnson et al., 2007).

The functional relevance of submes-MØs in defense against peritoneal bacterial infection and their response to peritoneal metastatic tumor growth are currently being addressed in Carlos Ardavín's lab.

8. Conclusions

1. Three main subpopulations of macrophages can be identified by WMI-CF imaging of the peritoneal submesothelial space: Tim4^{+} MHCII^{low}, Tim4^{+} MHCII^{high} and Tim4^{-} MHCII^{high} submes-MØs.
2. Differential Tim4 and Gata6 expression, and dependence on the chemokine receptor CCR2, support that Tim4^{+} MHCII^{low} and Tim4^{+} MHCII^{high} submes-MØs are resident embryonic macrophages, whereas Tim4^{-} MHCII^{high} submes-MØs are monocyte-derived.
3. Peritoneal *E. coli* infection promotes a change in submes-MØs morphology, involving the formation of three-dimensional extensions that penetrate between mesothelial cells, suggesting that *E. coli* triggers the activation of submes-MØs that might contribute to defense against bacterial infection.

Our data support the existence of a submesothelial macrophage barrier involved in defense against aggressions of the peritoneal cavity and, therefore, contribute to a better understanding of the peritoneal innate immune system, that is needed for the development of novel immunotherapy-based treatments of peritoneal infection and tumor metastasis.

9. Bibliography

Ahmed, R., Akira, S., Casadevall, A., Feinstone, W. H., Compans, R. W., Galan, J. E., Garcia-Sastre, A., & Malissen, B. (2020). *Current Topics in Microbiology and Immunology Volume 434 Series Editors*.

Ardavín, C., Alvarez-Ladrón, N., Ferriz, M., Gutiérrez-González, A., & Vega-Pérez, A. (2023). Mouse Tissue-Resident Peritoneal Macrophages in Homeostasis, Repair, Infection, and Tumor Metastasis. *Advanced Science*, 2206617.

Bain, C. C., & Jenkins, S. J. (2018). The biology of serous cavity macrophages. *Cellular Immunology*, *330*, 126–135.

Berberich, S., Förster, R., & Pabst, O. (2007). The peritoneal micromilieu commits B cells to home to body cavities and the small intestine. *Blood*, *109*, 4627–4634.

Buechler, M. B., Kim, K. W., Onufer, E. J., Williams, J. W., Little, C. C., Dominguez, C. X., Li, Q., Sandoval, W., Cooper, J. E., Harris, C. A., Junttila, M. R., Randolph, G. J., & Turley, S. J. (2019). A Stromal Niche Defined by Expression of the Transcription Factor WT1 Mediates Programming and Homeostasis of Cavity-Resident Macrophages. *Immunity*, *51*(1), 119-130.e5.

Capobianco, A., Cottone, L., Monno, A., Manfredi, A. A., & Rovere-Querini, P. (2017). The peritoneum: healing, immunity, and diseases. *The Journal of Pathology*, *243*(2), 137–147.

Chakarov, S., Lim, H. Y., Tan, L., Lim, S. Y., See, P., Lum, J., Zhang, X. M., Foo, S., Nakamizo, S., Duan, K., Kong, W. T., Gentek, R., Balachander, A., Carbajo, D., Bleriot, C., Malleret, B., Tam, J. K. C., Baig, S., Shabeer, M., … Ginhoux, F. (2019). Two distinct interstitial macrophage populations coexist across tissues in specific subtissular niches. *Science*, *363*(6432).

Ferriz, M., Vega-Pérez, A., Gutiérrez-González, A., Alvarez-Ladrón, N., & Ardavín, C. (2023). Whole-mount immunofluorescence imaging and isolation of mesothelium-bound immune cell aggregates during mouse peritoneal inflammation. *STAR Protocols*, *4*(1), 102079.

Gautier, E. L., Shay, T., Miller, J., Greter, M., Jakubzick, C., Ivanov, S., Helft, J., Chow, A., Elpek, K. G., Gordonov, S., Mazloom, A. R., Ma'Ayan, A., Chua, W. J., Hansen, T. H., Turley, S. J., Merad, M., Randolph, G. J., Best, A. J., Knell, J., … Benoist, C. (2012). Gene-expression profiles and transcriptional regulatory pathways that underlie the identity and diversity of mouse tissue macrophages. *Nature Immunology*, *13*(11), 1118–1128.

Gautier, E. L., Ivanov, S., Williams, J. W., Huang, S. C. C., Marcelin, G., Fairfax, K., Wang, P. L., Francis, J. S., Leone, P., Wilson, D. B., Artyomov, M. N., Pearce, E. J., & Randolph, G. J. (2014). Gata6 regulates aspartoacylase expression in resident peritoneal macrophages and controls their survival. *Journal of Experimental Medicine*, *211*(8), 1525–1531.

Harris, G., KuoLee, R., Xu, H. H., & Chen, W. (2019). Acute intraperitoneal infection with a hypervirulent Acinetobacter baumannii isolate in mice. *Scientific Reports*, *9*(1).

Hwee Ying Lim, A., Yng Lim, S., Kun Tan, C., & Jackson, D. G. (2018). Hyaluronan Receptor LYVE-1-Expressing Macrophages Maintain Arterial Tone through Hyaluronan-Mediated Regulation of Smooth Muscle Cell

Collagen LYVE-1 on macrophage engages HA on smooth muscle for collagen degradation. *Immunity*, *49*, 326–341.

Jackson, D. G., Prevo, R., Clasper, S., & Banerji, S. (2001). LYVE-1, the lymphatic system and tumor lymphangiogenesis. *Trends in Immunology*, *22*(6), 317–321.

Johnson, L. A., Prevo, R., Clasper, S., & Jackson, D. G. (2007). Inflammation-induced Uptake and Degradation of the Lymphatic Endothelial Hyaluronan Receptor LYVE-1. *Journal of Biological Chemistry*, *282*(46), 33671–33680.

Leendertse, M., Willems, R. J. L., Giebelen, I. A. J., Roelofs, J. J. T. H., van Rooijen, N., Bonten, M. J. M., & van der Poll, T. (2009). Peritoneal macrophages are important for the early containment of Enterococcus faecium peritonitis in mice. *Innate Immunity*, *15*(1), 3–12.

Liu, M., Silva-Sanchez, A., Randall, T. D., & Meza-Perez, S. (2021). Specialized immune responses in the peritoneal cavity and omentum. *Journal of Leukocyte Biology*, *109*(4), 717–729.

Mark Ansel K., R. B. S., C. G. J. (2002). *CXCL13 Is Required for B1 Cell Homing, Natural Antibody Production, and Body Cavity Immunity*.

Meza-Perez, S., & Randall, T. D. (2017). Immunological Functions of the Omentum. In *Trends in Immunology* (Vol. 38, Issue 7, pp. 526–536). Elsevier Ltd.

Nishi, C., Toda, S., Segawa, K., & Nagata, S. (2014). Tim4- and MerTK-Mediated Engulfment of Apoptotic Cells by Mouse Resident Peritoneal Macrophages. *Molecular and Cellular Biology*, *34*(8), 1512–1520.

Okabe, Y., & Medzhitov, R. (2014). Tissue-specific signals control reversible program of localization and functional polarization of macrophages. *Cell*, *157*(4), 832–844.

Reim, D., Rossmann-Bloeck, T., Jusek, G., Costa, O. P. da, & Holzmann, B. (2011). Improved host defense against septic peritonitis in mice lacking MyD88 and TRIF is linked to a normal interferon response. *Journal of Leukocyte Biology*, *90*(3), 613–620.

Salm, L., Shim, R., Noskovicova, N., & Kubes, P. (2023). Gata6+ large peritoneal macrophages: an evolutionarily conserved sentinel and effector system for infection and injury. In *Trends in Immunology* (Vol. 44, Issue 2, pp. 129–145). Elsevier Ltd.

Shi, C., & Pamer, E. G. (2011). Monocyte recruitment during infection and inflammation. *Nature Reviews Immunology 2011 11:11*, *11*(11), 762–774.

Smith, F. L., & Baumgarth, N. (2019). B-1 cell responses to infections. In *Current Opinion in Immunology* (Vol. 57, pp. 23–31). Elsevier Ltd.

Szender, J. B., Emmons, T., Belliotti, S., Dickson, D., Khan, A., Morrell, K., Khan, A. N. M. N., Singel, K. L., Mayor, P. C., Moysich, K. B., Odunsi, K., Segal, B. H., & Eng, K. H. (2017). Impact of ascites volume on clinical outcomes in ovarian cancer: A cohort study. *Gynecologic Oncology*, *146*(3), 491–497.

Uderhardt, S., Martins, A. J., Tsang, J. S., Lämmermann, T., & Germain, R. N. (2019). Resident Macrophages Cloak Tissue Microlesions to Prevent Neutrophil-Driven Inflammatory Damage. *Cell*, *177*(3), 541-555.e17.

van Baal, J. O. A. M., Van de Vijver, K. K., Nieuwland, R., van Noorden, C. J. F., van Driel, W. J., Sturk, A., Kenter, G. G., Rikkert, L. G., & Lok, C. A. R. (2017). The histophysiology and pathophysiology of the peritoneum. In *Tissue and Cell* (Vol. 49, Issue 1, pp. 95–105). Churchill Livingstone.

Vega-Pérez, A., Villarrubia, L. H., Godio, C., Gutiérrez-González, A., Feo-Lucas, L., Ferriz, M., Martínez-Puente, N., Alcaín, J., Mora, A., Sabio, G., López-Bravo, M., & Ardavín, C. (2021). Resident macrophage-dependent immune cell scaffolds drive anti-bacterial defense in the peritoneal cavity. *Immunity*, *54*(11), 2578-2594.e5.

Wynn, T. A., & Vannella, K. M. (2016). Macrophages in Tissue Repair, Regeneration, and Fibrosis. *Immunity*, *44*(3), 450–462.

Zhang, N., Kim, S. H., Gainullina, A., Erlich, E. C., Onufer, E. J., Kim, J., Czepielewski, R. S., Helmink, B. A., Dominguez, J. R., Saunders, B. T., Ding, J., Williams, J. W., Jiang, J. X., Segal, B. H., Zinselmeyer, B. H., Randolph, G. J., & Kim, K. W. (2021). Lyve1+ macrophages of murine peritoneal mesothelium promote omentum-independent ovarian tumor growth. *Journal of Experimental Medicine*, *218*(12).

10. Supplementary information

Table 1: Antibodies table.

Antibodies	Source
Anti-CD11b PE-Cy7-conjugate, clone M1/70 (1:3000)	eBioscience
Anti-CD90.2, PE-conjugate, clone 53-2.1 (1:500)	BD Biosciences
Anti-CD19, PE-conjugate, clone 1D3 (1:400)	BD Biosciences
Anti-Ly6G, PE-conjugate, clone 1A8 (1:200)	BD Biosciences
Anti-CD45, FITC-conjugate, clone 30-F11 (1:100)	BioLegend
Anti-MHC II (I-A/I-E), APC-conjugate, clone M5/114.15.2 (1:1000)	eBioscience
Anti-Tim4, BV421-conjugate, clone 21H12 (1:3000)	BD Biosciences
Anti-F4/80, APC-Cy7-conjugate, clone BM8 (1:200)	BioLegend
Anti-Lyve-1, Alexa Fluor 488-conjugste, clone ALY7 (FC 1:100; IHC 1:500)	eBioscience
Anti-Tim4, Alexa Fluor 647-conjugate, clone 21H12 (1:500)	BD Biosciences
Anti-MHCII, Alexa Fluor 594-conjugate, clone M5/114.15.2 (1:500)	BioLegend
Anti-Podoplanin, Alexa Fluor 488-conjugate, clone 8.1.1 (1:1000)	BioLegend
Anti-CD16/32, clone 2.4G2 (1:100)	BD Biosciences

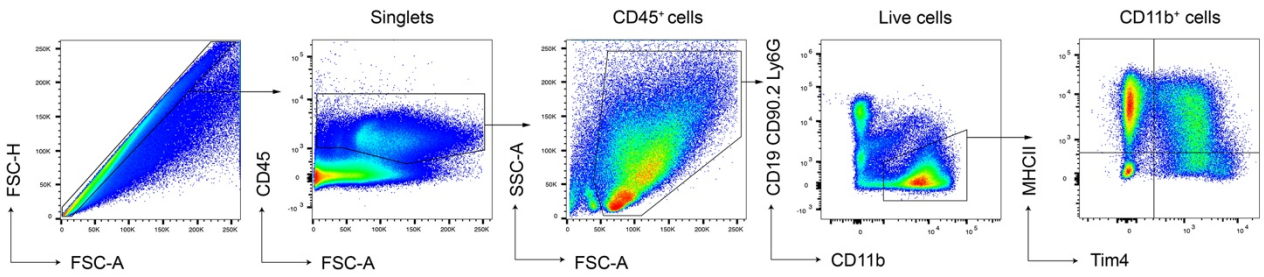

Figure 13: Gating strategy used for analyzing submesothelial MØ subpopulations.